SAGE-Hindawi Access to Research
International Journal of Electrochemistry
Volume 2011, Article ID 563427, 10 pages
doi:10.4061/2011/563427

Research Article

Photoelectrochemical Stability and Alteration Products of n-Type Single-Crystal ZnO Photoanodes

I. E. Paulauskas,[1] G. E. Jellison Jr.,[2] L. A. Boatner,[2,3] and G. M. Brown[4]

[1] *Department of Materials Science and Engineering, The University of Tennessee, Knoxville, TN 37996, USA*
[2] *Materials Science and Technology Division, Oak Ridge National Laboratory, Oak Ridge, TN 37831-6197, USA*
[3] *Center for Radiation Detection Materials and Systems, Oak Ridge National Laboratory, Oak Ridge, TN 37831-6056, USA*
[4] *Chemical Sciences Division, Oak Ridge National Laboratory, Oak Ridge, TN 37831-6119, USA*

Correspondence should be addressed to L. A. Boatner, boatnerla@ornl.gov

Received 24 November 2010; Accepted 22 January 2011

Academic Editor: Shen-Ming Chen

The photoelectrochemical stability and surface-alteration characteristics of doped and undoped n-type ZnO single-crystal photoanode electrodes were investigated. The single-crystal ZnO photoanode properties were analyzed using current-voltage measurements plus spectral and time-dependent quantum-yield methods. These measurements revealed a distinct anodic peak and an accompanying cathodic surface degradation process at negative potentials. The features of this peak depended on time and the NaOH concentration in the electrolyte, but were independent of the presence of electrode illumination. Current measurements performed at the peak indicate that charging and discharging effects are apparently taking place at the semiconductor/electrolyte interface. This result is consistent with the significant reactive degradation that takes place on the ZnO single crystal photoanode surface and that ultimately leads to the reduction of the ZnO surface to Zn metal. The resulting Zn-metal reaction products create unusual, dendrite-like, surface alteration structural features that were analyzed using x-ray diffraction, energy-dispersive analysis, and scanning electron microscopy. ZnO doping methods were found to be effective in increasing the n-type character of the crystals. Higher doping levels result in smaller depletion widths and lower quantum yields, since the minority carrier diffusion lengths are very short in these materials.

1. Introduction

The increasing demand for energy, coupled with the ongoing decreasing availability of fossil fuels and the undesirable consequences of their use, is driving the need to develop alternative fuels such as hydrogen—that is, fuels that can be both abundant and environmentally safe. Currently, the production of hydrogen is primarily achieved by either the steam reforming of methane, which results in CO_2 emissions, or water electrolysis, which currently requires the combustion of fossil fuels for the generation of electricity [1]. Neither method can be considered environmentally friendly. A more environmentally benign option for hydrogen generation is the use of photoelectrochemical (PEC) cells [1, 2]. These cells enable the clean production of hydrogen and oxygen though the photoassisted dissociation of water. This phenomenon was originally observed by Fujishima and Honda in 1972 when TiO_2 was irradiated with UV light [3]. Since that discovery, numerous studies have been conducted using semiconducting n-type oxides including titanium dioxide (TiO_2), strontium titanate ($SrTiO_3$), potassium tantalate ($KTaO_3$), and zinc oxide (ZnO), among others [1, 4–8]. These materials absorb solar energy or other optical energy sources and can drive the water electrolysis reaction ($2H_2O \xrightarrow{hv} 2H_2 + O_2$). However, no stable-electrode PEC system has yet been identified that can efficiently convert sunlight to hydrogen without an external applied bias.

The primary problem consists of finding electrode materials with band gaps that efficiently match the solar spectrum and band edges that allow for the direct photo-induced evolution of hydrogen and oxygen. Finding n-type materials that meet these criteria and that also exhibit the chemical stability required to avoid photoanodic dissolution in the PEC cell environment represents the fundamental

Table 1: ZnO single-crystals description.

Sample	Doping element	Doping Temperature (°C)	Time (hr)	Color	Carrier concentration ($\times 10^{17}$ cm^{-3})
(1) 197		None		Clear	0.55 ± 0.01
(2) 204	Te	1100	4	Clear	0.72 ± 0.21
(3) 201	Cd	1100	4	Clear	0.80 ± 0.01
(4) 203	Mg	1150	18	Dark orange	14 ± 1
(5) 199	Zn	1100	0.5	Dark orange	11 ± 1
(6) 198	Zn	1150	0.5	Dark orange	15 ± 1
(7) 158	Gd	Doping elements directly added to the melt		Light green	10 ± 4
(8) 151	In + Li	Doping elements directly added to the melt		Light blue	11 ± 5
(9) 152	Er	Doping elements directly added to the melt		Light green	14 ± 4
(10) 149	Ga + Li	Doping elements directly added to the melt		Blue	67 ± 4

materials challenge to achieving a significant advance in this area. While the metal oxide semiconductors $KTaO_3$, TiO_2, and $SrTiO_3$ have been shown to be chemically stable in the PEC cell electrolyte, their band gaps are too large for efficient solar energy conversion. The photoanodic chemical stability of ZnO is known to be lower than that of $SrTiO_3$, $KTaO_3$, or TiO_2, nevertheless, its use as a photoanode material has been investigated in earlier studies due to its relatively high level of photoactivity [9, 10]. With a band gap of 3.35 eV [2], ZnO has direct band absorption, and it exhibits n-type semiconducting characteristics even when doped—due to the presence of defects such as Zn on O antisites and oxygen vacancies that are formed during growth [11]. The photoanodic instability of ZnO in aqueous electrolytes [12, 13] has been noted previously. The present work significantly extends the results of the prior studies of ZnO stability by focusing on the details of the surface reaction and degradation characteristics associated with the photoanodic conditions. Both doped and undoped ZnO single-crystal photoanodes are investigated here—where the electronic properties of the single-crystal ZnO photoanodes have been modified through the use of various dopant elements and heat treatments. The role of these compositional variations in potentially improving both the ZnO surface stability in an operating PEC cell environment and the solar energy absorption properties has also been investigated.

2. Experimental Procedure

2.1. Sample Preparation. The ZnO singlecrystals used in this study were grown by Cermet, Inc., Atlanta, GA by utilizing a skull melting method, and the samples are described in Table 1. Samples denoted as 1 through 6 in Table 1 were doped by the thermochemical treatment of an undoped singlecrystal in a vacuum-sealed quartz ampoule in the presence of the vapor of the dopant metal. The remaining crystals in Table 1 (samples 7 through 10) were doped in the melt during growth under a high oxygen pressure (details of this melt growth system can be found in [14]). The ZnO sample plates were rectangular in shape with approximate dimensions of $10 \times 5 \times 0.5\,\text{mm}^3$ and were polished to a submicron surface finish.

The electrical contacts to the ZnO photoanodes used in the photoelectrochemical cell characterization studies were formed by coating one side of the plate with an InGa eutectic solution. A gold wire was then attached to the InGa-coated surface by soldering with an indium dot. This contact was subsequently covered with conductive silver paste to increase the mechanical strength of the contact. The area of the ZnO plate exposed to the PEC cell electrolyte was controlled by using an insulating epoxy mask. Contacts to the ZnO plates used in the Hall effect measurements were made by vapor depositing gold on four corners of the samples.

2.2. Electrochemical Measurements. Electrochemical studies were performed using a three-electrode H-shaped cell with a quartz window to permit efficient transmission of the UV portion of the light to the semiconducting photoanodes. A platinum strip served as the counter electrode and a saturated calomel reference electrode (SCE) was employed. The cell measurements were performed using a PAR Model 2263 Potentiostat/Galvanostat. Unless otherwise specified, the electrolyte used was 8.5 M NaOH at room temperature. The high concentration of NaOH is required so that the top of the conduction band of ZnO will be above or very close to the redox potential of the $2H_2O + 2e^- \Longleftrightarrow 2OH^- + H_2$ reaction. If the conduction band of ZnO is below the redox potential of the reaction given above, then the photoelectrochemical cell cannot operate without an external voltage.

2.2.1. Current versus Potential Response. Several types of current versus potential curves were measured. With the exception of the scan-rate-dependant curves, the scan rate used for all of the other measurements was 30 mV/s. Cyclic voltammetry was performed in going from the negative towards the positive potential and starting at the most negative potential value (unless otherwise specified). Current density versus applied potential (J-E) curves were measured both in the dark and under illumination, with

the illumination provided by a collimated 75 W Hg(Xe) arc lamp. According to the notation used here, anodic currents are positive, indicating that electrons are collected at the back contact of the semiconducting electrode. The cathodic currents are set as negative. These are associated with electrons flowing from the semiconducting electrode into the electrolyte, and are related to the observed surface reduction reactions.

To better understand the nature of the features exhibited by these curves, measurements were also made at various NaOH electrolyte concentrations (i.e., 0.01 M, 0.1 M, 1 M, 3 M, 5 M, 7 M, and 9 M)—and also by using a deaerated electrolyte. Additionally, some cyclic voltammetry curves were measured under dark conditions at various scan rates (i.e., 1, 5, 10, 20, 50, and 100 mV/s) in both a quiescent and stirred electrolyte.

2.2.2. Photocurrent Quantum Yield. Two different types of photocurrent quantum yield (QY) measurements were performed—one consisting of measuring the external QY as a function of the wavelength and the other by making measurements as a function of time at a given wavelength. For both types of measurements, the potential in the PEC cell was held at 0 V versus SCE.

The illumination system consisted of an Xe arc lamp and a single-pass monochromator with a 5 nm bandwidth. A BG-3 glass filter was used on the entrance slit of the monochromator to reduce stray-light effects. The spot size was ∼1.5 mm in diameter. For the spectral QY measurements, the dwell time between the points was set to 1 and 100 sec to establish possible time-related effects. The time-dependent QY measurements were performed at wavelengths of 260, 350, and 370 nm. A detailed description of the setup used for both types of QY measurements can be found in [15]. Transmission measurements at wavelengths between 350 and 800 nm were performed for some of the ZnO single crystals by using a Perkin Elmer Instruments Lambda 900 Spectrometer. Scanning electron microscope (SEM) images and energy dispersive X-ray spectroscopy (EDS) data were taken using a Hitachi S-3400N system.

3. Results and Discussion

3.1. Electrochemical Measurements

3.1.1. Current versus Potential Behavior. Figure 1 shows the J-E curves both in the dark and under illumination for sample 4 (see Table 1). The small photoresponse is, in part, attributable to the low intensity of the incident illumination above the ZnO band gap, $E_g = 3.4$ eV (365 nm). In this figure, it can also be seen that, as the potential was made more positive from a starting potential of −2.1 V versus SCE, an anodic peak (feature F) with a maximum at approximately −1.5 V versus SCE was observed—regardless of the presence of light. Similarly, when the voltage sweep direction was reversed, a cathodic peak (feature D) was observed at approximately −1.72 V versus SCE.

3.1.2. Electrode Surface Degradation Conditions. Visual inspection of the electrode during these measurements indicated the formation of a surface degradation product during the cathodic peak currents (indicated as "region D" in Figure 1). This product began to dissolve as the anodic peak currents were initiated (region F), and it appeared to be completely dissolved when the maximum peak current was reached. Bubbles formed at the electrode surface when the sweeping potential was ≤2 V versus SCE (region E). Changes in the direction of the cyclic sweep did not generate behavioral differences in the observed features. Additionally, the peaks were not affected by the presence of oxygen in the electrolyte. However, when the cyclic voltammetry sweep was limited to potentials between ∼ −1.6 and 1 V versus SCE, which omits the cathodic peak in the curve, neither the anodic nor the cathodic peaks were observed (see Figure 2). Furthermore, a voltage sweep from −1.5 to −2.1 V also showed no cathodic peak.

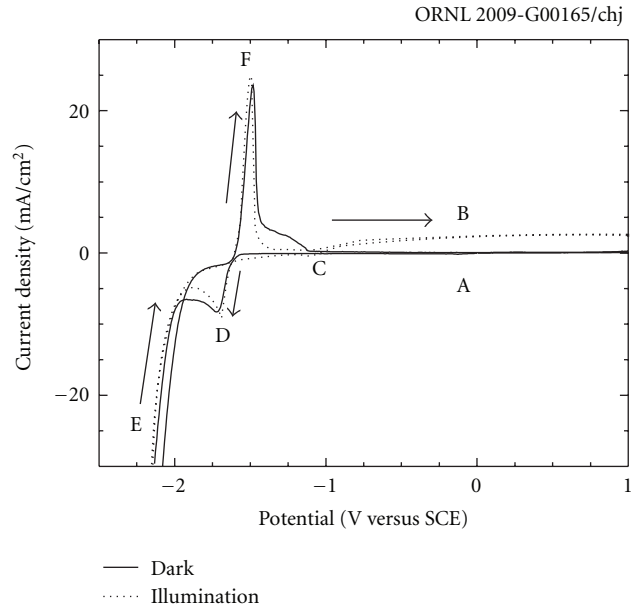

Figure 1: Current density versus applied potential curves for ZnO single-crystal electrode sample no. 4 (see Table 1) in the dark (solid line) and under illumination (dotted line). Regions A and B are reverse biased, showing photocurrent (B) under illumination or no current (A) in the dark. Position C is flat band, D is the cathodic peak, and F is the anodic peak. Bubbles formed at the electrode in region E. The arrows are used to emphasize the direction of the cyclic potential sweep.

The presence of these peaks, as well as an increase in the surface roughness of the ZnO electrodes after the cyclic voltammetry scans, indicated that significant chemical reactions at the ZnO-electrolyte interface had taken place that were responsible for the dissolution of the ZnO electrode into the electrolyte. Furthermore, the absence of the anodic peak in the scan between −1.6 and 1 V versus SCE, shows that this peak is related to the oxidation of the surface product that was generated during the cathodic peak.

The effect of varying the NaOH concentration on the J-E behavior of the samples can be seen in Figure 3. The peak current was found to increase with increasing

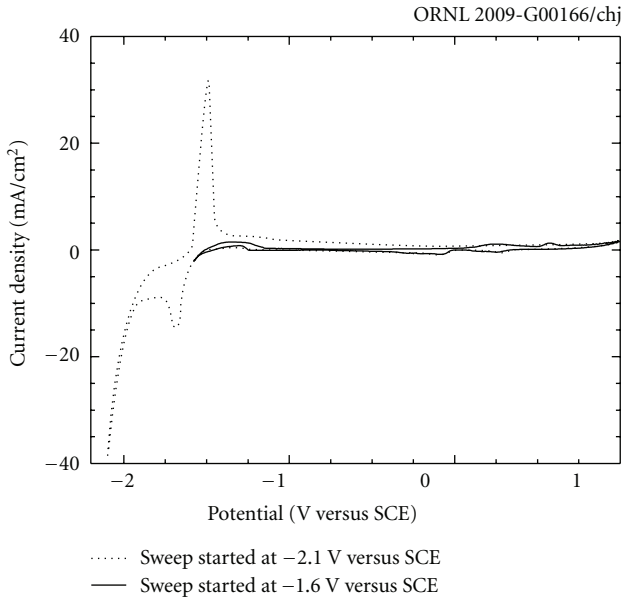

Figure 2: Current density versus applied potential curves for ZnO single-crystal electrode sample 4 (see Table 1) measured in the dark. Neither the cathodic, or anodic peaks are observed if the scan is started at a higher potential than the cathodic peak.

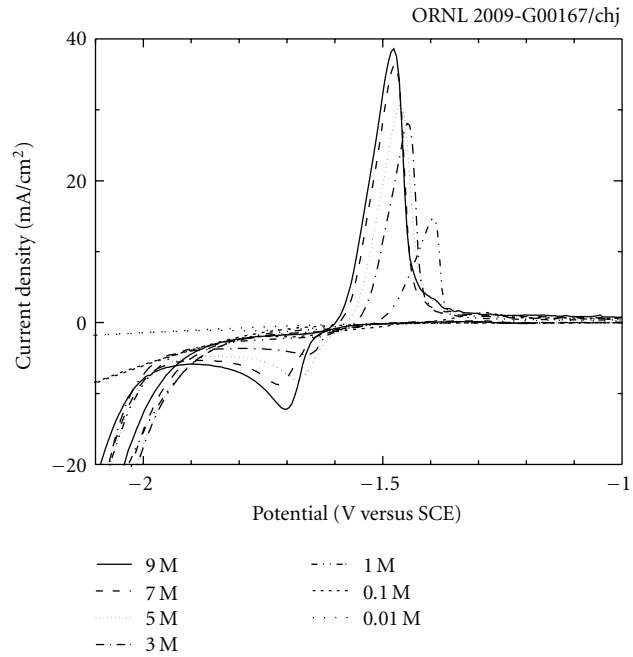

Figure 3: Current versus applied potential behavior of ZnO single-crystal electrode sample 4 as a function of the NaOH concentration in the electrolyte.

NaOH concentration. The "flat" cathodic currents are a consequence of the low conductivity of the electrolyte when the concentration was 0.01 M and 0.1 M NaOH. Additionally, the peak potential was found to become more negative as the NaOH concentration increased with a slope of approximately 120 mV per decade change in concentration between 0.01 M and 5 M NaOH (Figure 4). At this OH^- concentration the assumption of quasiequilibrium is a reasonable approximation, and the 120 mV slope suggests the ratio of OH^- to electrons involved in the rate limiting step leading to this anodic peak is 2. An equilibrium and/or saturation value appears to be reached at sufficiently high NaOH concentrations ($\geq$7 M NaOH).

The scan-rate dependence of the cyclic voltammetry curves measured in a quiescent and a stirred electrolyte indicated that the currents increased with the scan rate (Figure 5). This tendency is expected when a diffusion layer is involved in the charge or mass transfer process, and it can be understood in terms of the time spent at each potential of the scan and the time available for the formation of a diffusion layer. This effect became more noticeable via the overall increase in the current that was measured when the electrolyte was stirred (Figure 5(b))—as opposed to when it was quiescent (Figure 5(a)). The peak of the current densities in quiescent conditions as a function of the square root of the scan rate is shown in Figure 6, and this is consistent with the well-known Randles-Sevcik equation for linear sweep voltammetry [16]. The least squares fits are also shown (R^2 = 0.98 for both fits). This linearity suggests that the reactions taking place at the electrode surface are subject to a diffusion-controlled process where the anodic currents are very likely

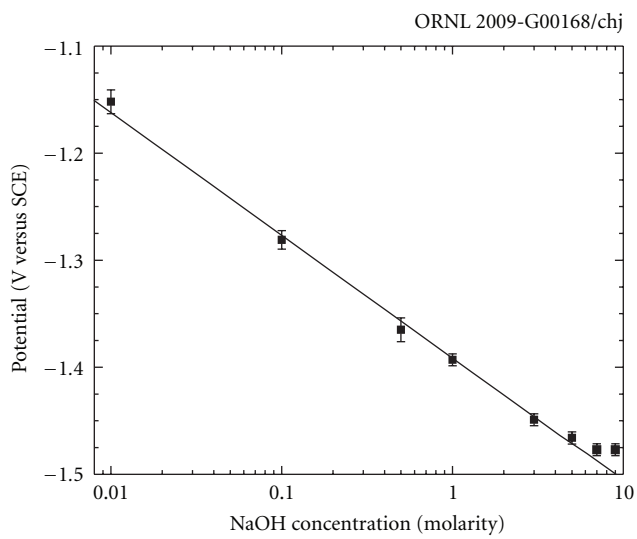

Figure 4: Peak potential as a function of the NaOH concentration in the electrolyte for ZnO electrode sample 4. The solid line is a least squares fit to the data points with a slope of 120 mV/decade, indicating a two-electron process.

being limited by the inward flow of water and/or hydroxyl ions (OH^-) and the outward flow of the reacting species from the electrode through the layer of the electrochemically generated species.

3.1.3. Altered Surface Layer Characteristics. The nature of the electrode surface alteration process was studied by holding

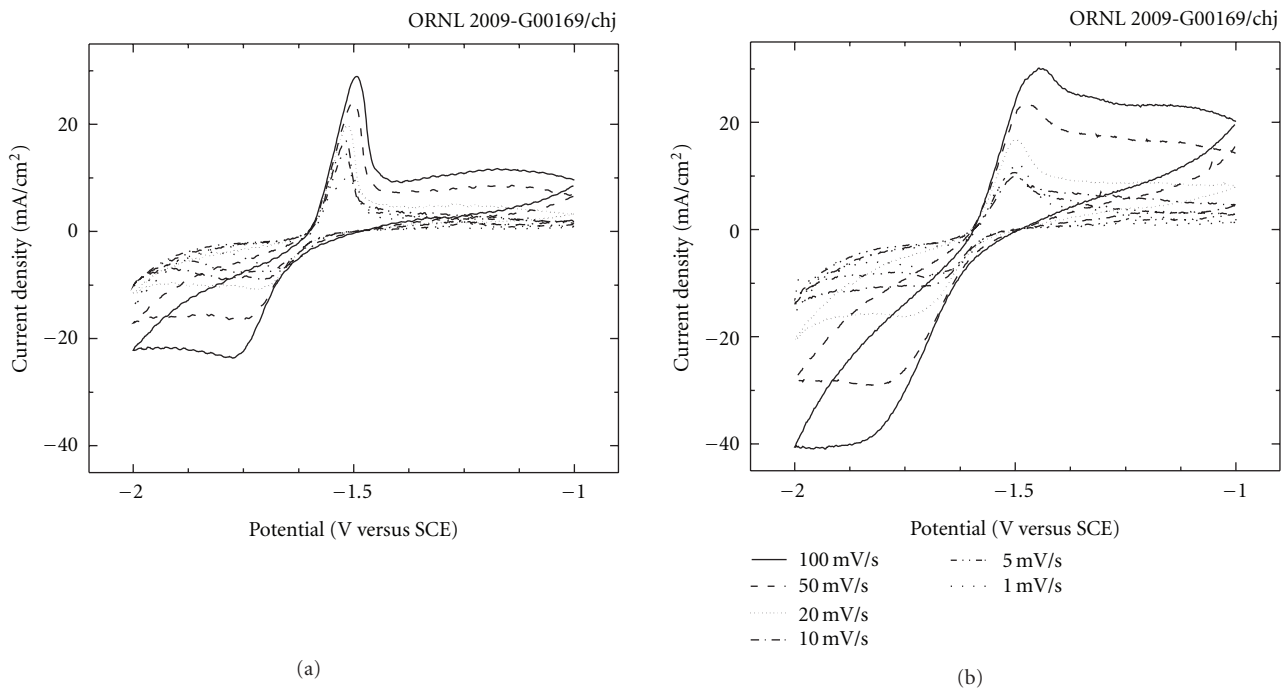

Figure 5: Current versus applied potential curves for ZnO electrode sample 4 at various scan rates in a quiet (a) and stirred (b) electrolyte.

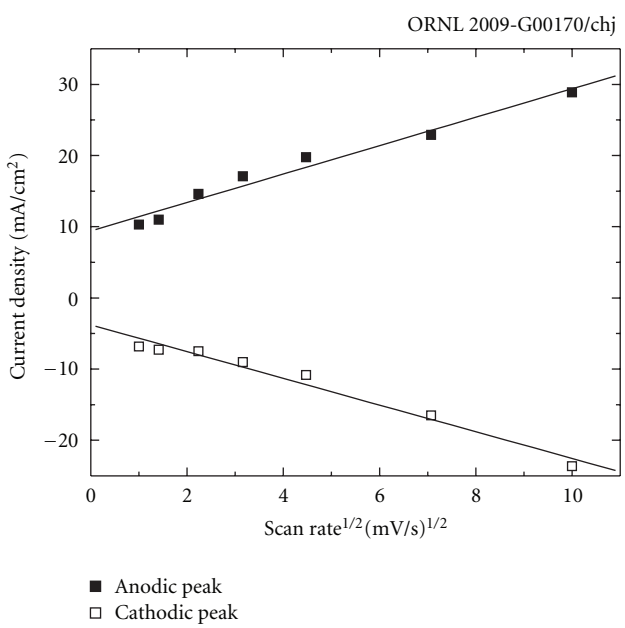

Figure 6: Anodic and cathodic peak current densities from Figure 5(a) as a function of the square root of the scan rate. The lines show a least squares fit to the data with an $R^2 = 0.98$.

a ZnO electrode at the cathodic peak potential for 17 hrs. The resulting surface product was metallic gray, and an X-ray powder diffraction examination indicated that the altered surface layer consisted primarily of Zn metal—with minor traces of ZnO (Figure 7). Figures 8–10 show scanning electron microscopy (SEM) images of the structures obtained at the surface of the electrode treated as noted above. Figure 8 shows the beginning stages of the Zn metallic growth after only 1 min of reaction time. It was not possible to estimate the Zn/O ratios by EDS at this level due to the high magnification needed to observe the surface details. Figure 9(a) shows a low-magnification view of the general electrode surface after a 17-hour reaction time in the cell. The structure of the altered surface layer consists of a series of "star-shaped" dendrite-like crystals that are loosely bound to form a porous layer. Other structures indicating the dendritic growth of the crystals were also observed (see Figure 9(b)). EDS results indicated that these crystals consisted primarily of Zn metal—but with some traces of oxygen. Table 2 shows the atomic percent (at%) compositions estimated by EDS analysis of the structures indicated in Figure 10. These results clearly show the presence of nonstoichiometric oxygen in some regions of the primarily metallic Zn structures found on the altered ZnO electrode surface.

Table 2: Atomic percent composition estimated by energy dispersive X-ray spectroscopy from Figure 10.

	Zn	O
a	60	40
b	68	32
c	79	21

Based on these findings, it is possible to correlate the regions A, B, C, D, E, and F of the J-E curve indicated in Figure 1 with the specific processes taking place at the

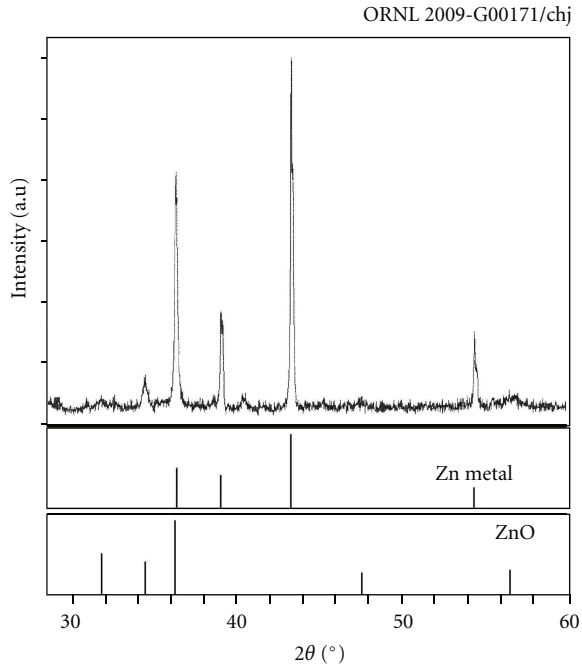

Figure 7: X-Ray diffraction pattern of the altered surface product generated during the reduction reaction of a ZnO single-crystal PEC cell electrode showing the formation of metallic zinc on the photoanode surface. Weak X-ray diffraction peaks from ZnO are also present.

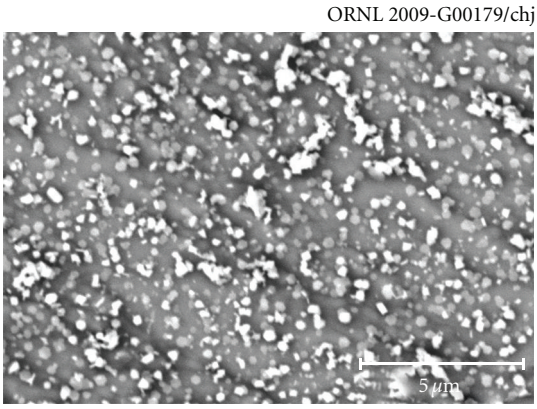

Figure 8: Early-onset growth of small metallic zinc particles on the single-crystal ZnO electrode surface. The cell operation/reduction time was 1 min.

ZnO electrode solution interface. In regions A and B, the potential is in the reversed bias condition and away from the flat-band potential, V_{fb}, which is located at approximately -0.9 V versus SCE in this electrolyte [17]. If the sample is not illuminated (A), then there is virtually no majority carrier current (injection, due to electrons), and only a small amount of minority carrier current (saturation, due to holes). Upon illumination, the minority carrier current increases, mostly from electron-hole pairs generated within the depletion region (it will be shown later that the part of the device beyond the depletion region is a very inefficient collector of electron-hole pairs, due primarily to minority carrier recombination).

As the potential becomes more negative and approaches V_{fb}, the bias generating the depletion width is reduced. Since most of the photocurrent comes from the depletion region, it starts to decrease as the injection current increases until it becomes zero (region C) at V_{fb}. As the potential becomes more negative than V_{fb}, very little current is observed since the potential must first overcome the kinetic activation barrier or over potential. As the potential is further reduced, the cathodic peak near -1.72 V versus SCE is observed (region D). As previously noted, these currents are related to the reduction of Zn^{+2} to $Zn^{0}(s)$ at the semiconductor-electrolyte interface. Once all the available ZnO on the semiconductor surface has been converted to Zn, then this reaction stops, reducing the current. Studies by Cai and Park have observed a similar peak in the electrochemical behavior of Zn metal in alkaline solutions [18]. Accordingly, it is possible to establish that the cathodic currents are the result of either or both of the following two reactions:

$$\begin{aligned} \text{ZnO} + \text{H}_2\text{O} + 2\text{e}^- &\longrightarrow \text{Zn} + 2\text{OH}^-, \\ \text{Zn(OH)}_2 + 2\text{e}^- &\longrightarrow \text{Zn} + 2\text{OH}^-. \end{aligned} \tag{1}$$

As the potentials are swept in a more negative direction below the cathodic peak, the cathodic current increases exponentially (E), where the current is given by

$$J(V) = J_o * \exp\left(\frac{-e(V - Vo)}{E_a}\right). \tag{2}$$

Equation (2) is of the same form as the Tafel Equation [16] so it is reasonable to associate this with the formation of hydrogen at the metallic zinc-solution interface. It is also possible that the zinc and/or the ZnO is being dissolved at this high negative potential. This is also consistent with the bubbles observed during these measurements. From Figure 3, it can be seen that when the NaOH concentration in the electrolyte is between 1 and 9 M, the slopes of the cathodic current do not change. The activation energy for this reaction is $E_a = 0.1$ eV.

When the direction of the potential sweep is changed and the potentials are made more positive, the cathodic currents are followed by region F that includes the anodic peak. From an inspection of the semiconductor during the cyclic sweeping, it is known that Zn metal is present at the surface of the electrode when the anodic currents start to rise—indicating that the source of the anodic current in region F is associated with the reoxidation of Zn. Cai and Park have attributed the increase in the anodic current in Zn electrodes to the formation of the zincate ions by means of the overall reaction [18, 19]

$$\text{Zn} + 4\text{OH}^- \longrightarrow \text{Zn(OH)}_4{}^{2-} + 2\text{e}^-. \tag{3}$$

It is suggested that this is a "step reaction" involving the formation of various surface zincate complex ions such as $Zn(OH)^-$ and $Zn(OH)_3{}^-$. In pure Zn electrodes, the reaction is expected to be limited by the inward flux of OH^- into the

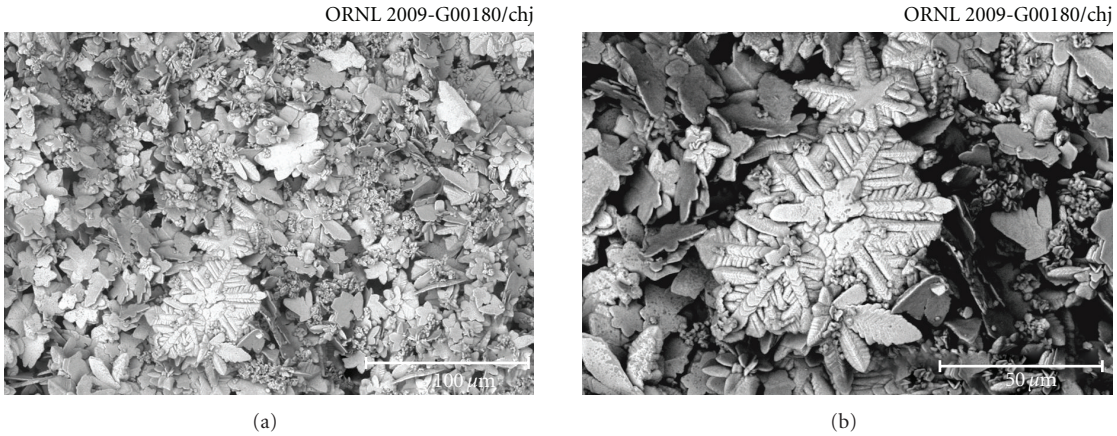

Figure 9: Metallic Zn crystal layer formed at the surface of a ZnO single-crystal photoanode after 17 hours of operation in a photoelectrochemical cell. (a) An overall low magnification view showing the porous nature of the altered surface layer. (b) A detailed view showing the Zn metal dendritic growth morphology.

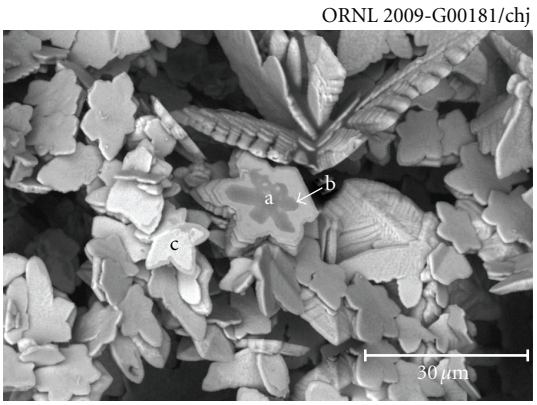

Figure 10: SEM micrograph of primarily metallic Zn crystal structures formed at the surface of a ZnO electrode after electrochemical reduction under PEC cell operation for 17 hrs. The darker regions indicate areas with a higher oxygen concentration. The compositional results obtained from an EDS analysis of the indicated regions a, b, and c are shown in Table 2. The hexagonal symmetry of metallic zinc is reflected in the shape of the dendrite-like plates that form in a repetitive layered structure as shown in the micrograph.

reaction site. However, in our ZnO crystals, the reaction may also be limited by the availability of Zn metal at the interface. This may account for the overlapping of the curves at 1, 5, and 10 mV/s in Figure 5(b). Additionally, as the potentials are made more positive than the peak value, the zincate ions can apparently become saturated and precipitate at the interface as a very loose $ZnO_{1-x}(OH)_{2x}$ adsorbed species. This may account for the presence of partially oxidized Zn that forms as indicated by the EDS data. However, the surface interactions between the ZnO crystal and the electrolyte at such negative potentials may well be more complicated than this, and further study is necessary to fully understand the surface kinetics reactions involved as a result of these applied potentials.

3.2. Carrier Concentration. Table 1 lists the doping concentrations determined from Hall effect measurements of the various n-type ZnO single crystals. These carrier concentrations indicate that the doping levels are relatively high—even for the undoped ZnO, which had a carrier concentration of $\sim 5.5 \times 10^{16}\,\mathrm{cm}^{-3}$. Neither the carrier concentration nor the color of the samples was dramatically affected when the ZnO crystals were thermochemically treated with Cd and Te metal vapor. In fact, the carrier concentration between the undoped and the Te-doped, and between the Cd- and the Te-doped crystals were the same within the experimental error. However, the Mg- and Zn-treated crystals did exhibit a change in color (from clear to dark orange), and the carrier concentration increased by more than an order of magnitude. The crystals doped during growth exhibited carrier concentrations in the range of $10^{18}\,\mathrm{cm}^{-3}$, which is near degeneracy.

3.3. Photocurrent Quantum Yield. ZnO electrode spectral quantum yield (QY) results are presented in Figure 11. The shape of the QY curve is consistent with the results of previous work [15], and it is related to the absorption coefficient and, hence, the penetration depth of light in ZnO. The drop in the QY near the band edge energy was not as sharp as expected for a direct band semiconductor due to the ± 5 nm bandwidth of the monochromator. The feature observed immediately before this drop is an effect of the exciton absorption just below the band edge [20].

The height of the QY curve decreases as the carrier concentration increases. Figure 11(a) shows that the highest QY was observed for the undoped crystal (sample 1), followed by samples 2 and 3 that had statistically identical carrier concentration values. Samples 5 and 6 were both heat treated with Zn metal vapor for 30 min, and a slightly higher carrier concentration was obtained when the temperature was held 50°C higher (sample 6). This change in carrier concentration was sufficient to produce a drop of ~20% in the QY.

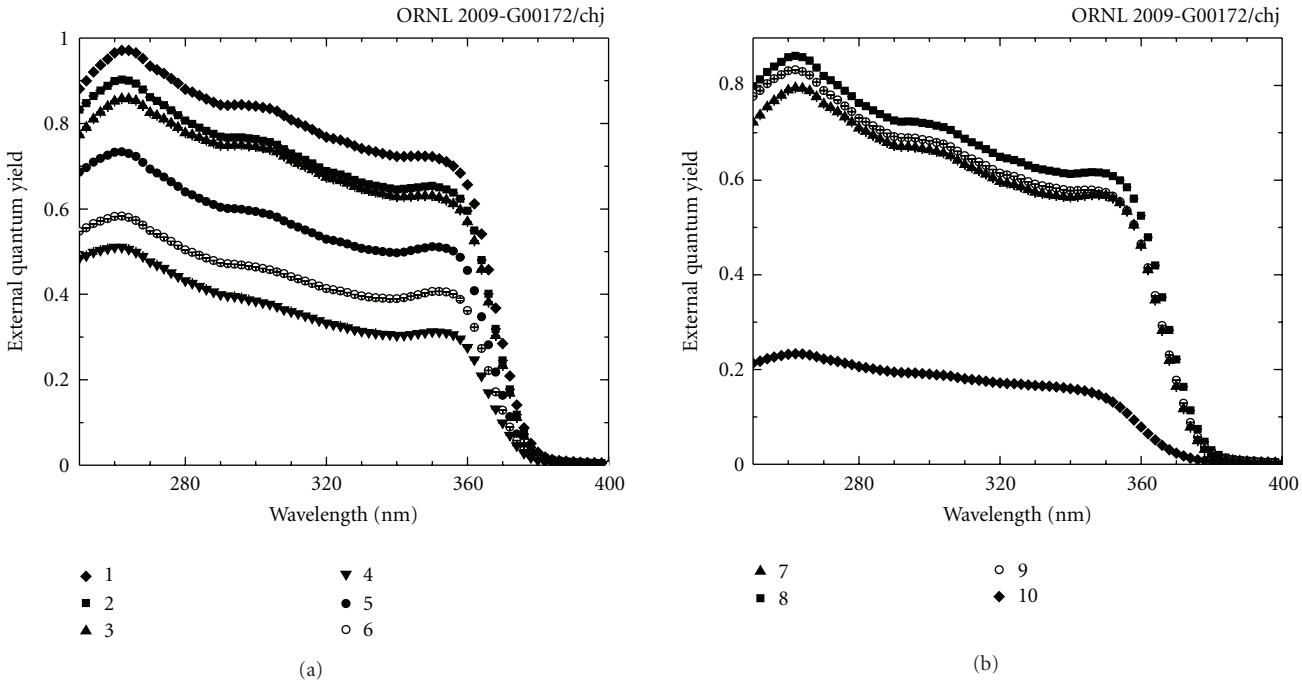

Figure 11: Spectral photocurrent quantum yield of the various single-crystal ZnO semiconducting photoanodes for (a) the thermochemically doped (1)–(6) samples and (b) the samples (7)–(9) doped in the melt during growth. The quantum yield correlates well with carrier concentration (see Table 1), where lower carrier concentrations result in a larger quantum yield.

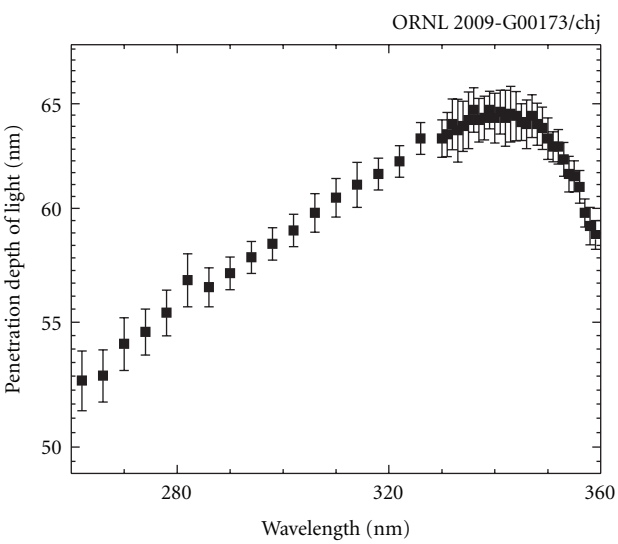

Figure 12: The optical penetration depth δ of light as a function of the wavelength for ZnO, where the optical absorption coefficient $\alpha = 1/\delta$. Data replotted from [19].

From the group of ZnO samples doped during growth, samples 7, 8, and 9 exhibited a similar QY (Figure 11(b))—consistent with the fact that the measured carrier concentrations are statistically the same. The lowest measured QY was found for sample 10, which exhibited the highest overall carrier concentration. Time-dependant measurements of the QY indicated that the ZnO photoanodes exhibited a small time dependence as compared to that observed for degenerate $KTaO_3$ in the same type of photoelectrochemical cell environment [15, 21]. The longest relaxation time in the QY occurred at a wavelength of 260 nm, where it required ~30 sec to equilibrate. However, the total changes in the QY values were less than 2% for all of the wavelengths tested.

3.4. Optical Measurements and Quantum Yield. A study was also made of the correlation of the ZnO/cell properties and the optical absorption characteristics. Figure 12 shows the penetration depth of light δ for ordinary polarization ($\delta = 1/\alpha$, where α is the optical absorption coefficient) in ZnO as a function of the wavelength in the UV region [20]. Since all of the crystals were oriented with the c-axis perpendicular to the surface, the ordinary optical functions are used. As shown in Figure 12, there is a linear increase in the penetration depth between 260 and 340 nm where the 340–350 nm wavelength light is absorbed (~10 nm deeper than the 260 nm light). The depletion width for the ZnO electrodes was estimated using an ideal one-sided abrupt junction approximation [22] represented by the following equation:

$$W = \sqrt{\frac{2\varepsilon_s}{qN}\left(V_{\mathrm{bi}} - \frac{2kT}{q}\right)}, \tag{4}$$

where ε_s represents the static dielectric constant (7.61 from [23]), q the electron charge, N the carrier concentration, k Boltzmann's constant, and T the temperature in Kelvin. Figure 13 shows the ideal depletion widths for three built-in voltages (V_{bi}) as a function of the carrier concentration.

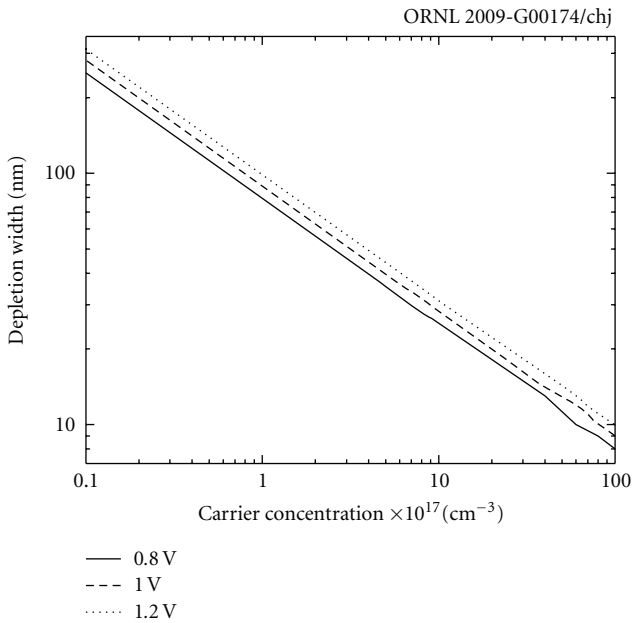

Figure 13: The estimated depletion width for ZnO single crystals as a function of the carrier concentration at the semiconductor-electrolyte interface for three different built-in potentials (V versus SCE).

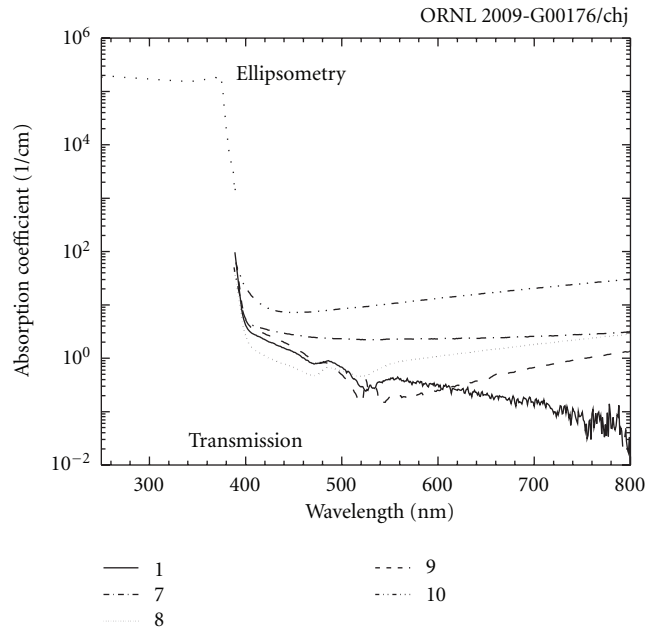

Figure 14: Absorption coefficient as a function of wavelength for the indicated doped and undoped ZnO single crystals described in Table 1.

Comparing the values of W and the penetration depth of light is useful in understanding the decay of the QY observed between 260 and 350 nm. From Figure 12, it is observed that the light penetration depth is ~55 nm and the depletion depth for sample 1 is ~110 nm. Consequently, ~85% of the photons at this wavelength are absorbed within the depletion region, where the QY is at its highest value. As the wavelength increases, the penetration depth of the light also increases, which results in fewer photons being absorbed within the depletion region, decreasing the quantum yield. The consistent decay of the QY with the penetration depth of light at this larger depletion width suggests that very few of the electron-hole pairs generated beyond the depletion width are collected by the external circuit, indicating a large number of recombination centers in the material. In addition, recombination can occur at the electrolyte/ZnO surface, further reducing the QY. This is not unexpected due to the high carrier concentration that is present for even an undoped ZnO single crystal.

The effect of the high carrier concentration can also be observed in Figure 14 where ellipsometry and optical transmission data were used to calculate the absorption coefficient of ZnO for samples 7 to 10. The ellipsometry data (upper curve from 250 to 400 nm) was replotted from [20] for use in this figure, since doping does not appreciably affect the optical properties above the band edge. However, the transmission data (lower part of the curve between 400 and 800 nm) was found to change significantly as a function of the carrier concentration. The absorption coefficient of the undoped crystal decreases as a function of wavelength in this range. On the other hand, the absorption coefficient of samples 7, 8, and 9 (which have equivalent carrier concentrations) seems to reach higher and similar values at the longer wavelengths. The absorption coefficient of sample 10 (the most heavily doped) is the highest through the entire wavelength range. This behavior in the absorption is caused by free carrier absorption; however, at these short wavelengths, it was not possible to establish the origin of the free carrier absorption (acoustic phonons, optical phonons, and/or ionized impurities), and the error limits on the measurements preclude the drawing of any further conclusions. Sharp lines exhibited by samples 1, 8, and 9 between 480 and 560 nm are apparently indicators of impurity bands.

4. Conclusions

Cyclic voltammetry results for ZnO PEC cell electrodes operated in a NaOH electrolyte show the presence of various regions on the cyclic voltammetry curve that have been correlated with specific chemical reactions that occur at the ZnO electrode. Specifically, a cathodic peak is observed at −1.75 V versus SCE, which corresponds to the reduction of ZnO to Zn metal and hydroxyl ions, and an anodic peak is observed at −1.4 V versus SCE, which corresponds to the reaction of Zn metal with the hydroxyl ions to form zincate ions. Both reactions involve two electrons. Cyclic voltammetry measurements as a function of scan rate indicate that the reactions at the electrode/electrolyte surface are diffusion controlled, where the anodic currents are limited by the inward flow of water and/or hydroxyl ions and the cathodic currents are limited by the outward flow of material from the electrode through a surface layer. When the ZnO electrode is maintained at the cathodic peak, the

altered surface layer that forms consists primarily of metallic Zn metal plus minor traces of ZnO. As this altered layer thickens the metallic zinc forms a distinctive dendrite-like structure. This layer begins to dissolve during the anodic current region, and it has dissolved completely when the peak of the anodic curve is reached.

The decrease in quantum yield (QY) observed between 260 and 350 nm is a direct result of the increase in the penetration depth of light, since a larger penetration depth corresponds to fewer electron-hole pairs being formed in the depletion region. Higher carrier concentrations result in a decreased depletion width, and therefore, a decreased QY. Higher carrier concentrations also result in larger optical absorption coefficients for wavelengths longer than the direct band edge (~365 nm).

Acknowledgments

This paper was sponsored by the Division of Materials Science and Engineering, Office of Basic Energy Sciences, US Department of Energy. The authors give special thanks to Joanne Ramey, Jim Kolopus, and Larry Walker for their help in various aspects of this work and to N. S. Lewis of Cal Tech for his suggestions and early encouragement.

References

[1] T. Bak, J. Nowotny, M. Rekas, and C. C. Sorrell, "Photoelectrochemical hydrogen generation from water using solar energy. Materials-related aspects," *International Journal of Hydrogen Energy*, vol. 27, no. 10, pp. 991–1022, 2002.

[2] N. M. X. Tan, P. E. Laibinis, S. T. Nguyen, J. M. Kesselman, C. E. Stanton, and N. S. Lewis, "Principles and applications of semiconductor photoelectrochemistry," in *Progress in Inorganic Chemistry*, K. D. Karlin, Ed., vol. 41, p. 21, John Wiley & Sons, New York, NY, USA, 1994.

[3] A. Fujishima and K. Honda, "Electrochemical photolysis of water at a semiconductor electrode," *Nature*, vol. 238, no. 5358, pp. 37–38, 1972.

[4] K. Rajeshwar, "Hydrogen generation at irradiated oxide semiconductor-solution interfaces," *Journal of Applied Electrochemistry*, vol. 37, no. 7, pp. 765–787, 2007.

[5] J. G. Mavroides, J. A. Kafalas, and D. F. Kolesar, "Photoelectrolysis of water in cells with $SrTiO_3$ anodes," *Applied Physics Letters*, vol. 28, no. 5, pp. 241–243, 1976.

[6] M. S. Wrighton, A. B. Ellis, P. T. Wolczanski, D. L. Morse, H. B. Abrahamson, and D. S. Ginley, "Strontium titanate photoelectrodes. Efficient photoassisted electrolysis of water at zero applied potential," *Journal of the American Chemical Society*, vol. 98, no. 10, pp. 2774–2779, 1976.

[7] A. J. Bard and M. S. Wrighton, "Thermodynamic potential for the anodic dissolution of n-type semiconductors," *Journal of the Electrochemical Society*, vol. 124, no. 11, pp. 1706–1710, 1977.

[8] H. P. Maruska and A. K. Ghosh, "Photocatalytic decomposition of water at semiconductor electrodes," *Solar Energy*, vol. 20, no. 6, pp. 443–458, 1978.

[9] M. V. Rao, K. Rajeshwar, V. R. P. Verneker, and J. DuBow, "Photosynthetic production of H_2 and HO_2 on semiconducting oxide grains in aqueous solutions," *Journal of Physical Chemistry*, vol. 84, no. 15, pp. 1987–1991, 1980.

[10] S. N. Frank and A. J. Bard, "Heterogeneous photocatalytic oxidation of cyanide and sulfite in aqueous solutions at semiconductor powders," *Journal of Physical Chemistry*, vol. 81, no. 15, pp. 1484–1488, 1977.

[11] Ü. Özgür, Ya. I. Alivov, C. Liu et al., "A comprehensive review of ZnO materials and devices," *Journal of Applied Physics*, vol. 98, no. 4, Article ID 041301, 103 pages, 2005.

[12] J. Doménech and A. Prieto, "Stability of ZnO particles in aqueous suspensions under UV illumination," *Journal of Physical Chemistry*, vol. 90, no. 6, pp. 1123–1126, 1986.

[13] H. Gerischer and N. Sorg, "Chemical dissolution of zinc oxide crystals in aqueous electrolytes—an analysis of the kinetics," *Electrochimica Acta*, vol. 37, no. 5, pp. 827–835, 1992.

[14] J. S. Neal, N. C. Giles, X. Yang et al., "Evaluation of melt-grown, ZnO single crystals for use as alpha-particle detectors," *IEEE Transactions on Nuclear Science*, vol. 55, no. 3, pp. 1397–1403, 2008.

[15] I. E. Paulauskas, J. E. Katz, G. E. Jellison Jr., N. S. Lewis, and L. A. Boatner, "Photoelectrochemical studies of semiconducting photoanodes for hydrogen production via water dissociation," *Thin Solid Films*, vol. 516, no. 22, pp. 8175–8178, 2008.

[16] A. J. Bard and L. R. Faulkner, *Electrochemical Methods: Fundamentals and Applications*, John Wiley & Sones, New York, NY, USA, 2nd edition, 2001.

[17] A. E. Bohe, J. R. Vilche, K. Jüttner, W. J. Lorenz, W. Kautek, and W. Paatasch, "An electrochemical impedance spectroscopy study of passive zinc and low alloyed zinc electrodes in alkaline and neutral aqueous solutions," *Corrosion Science*, vol. 32, no. 5-6, pp. 621–633, 1991.

[18] M. Cai and S. M. Park, "Spectroelectrochemical studies on dissolution and passivation of zinc electrodes in alkaline solutions," *Journal of the Electrochemical Society*, vol. 143, no. 7, pp. 2125–2131, 1996.

[19] M. Cai and S. M. Park, *Journal of the Electrochemical Society*, vol. 143, p. 3900, 1996.

[20] G. E. Jellison Jr. and L. A. Boatner, "Optical functions of uniaxial ZnO determined by generalized ellipsometry," *Physical Review B*, vol. 58, no. 7, pp. 3586–3589, 1998.

[21] I. E. Paulauskas, J. E. Katz, G. E. Jellison Jr., N. S. Lewis, L. A. Boatner, and G. M. Brown, "Growth, characterization, and electrochemical properties of doped n-type $KTaO_3$ photoanodes," *Journal of the Electrochemical Society*, vol. 156, no. 5, pp. B580–B587, 2009.

[22] S. M. Sze, *Physics of Semiconductor Devices*, John Wiley & Sons, New York, NY, USA, 2nd edition, 1981.

[23] H. Yoshikawa and S. Adachi, "Optical constants of ZnO," *Japanese Journal of Applied Physics*, vol. 36, no. 10, pp. 6237–6243, 1997.